Enhanced Stability and Mobility of Solution-Processed Oxide Thin-Film Transistors with Bilayer Terbium-incorporated Indium Oxide Channel

Penghui He,[1,2] Chunchun Ding,[3] Xuming Zou,[1,2] Guoli Li,[1,2], Wei Hu,[1,2] Chao Ma,[4] Denis Flandre,[1,5] Benjamín Iñíguez,[6] Lei Liao,[1,2,a)] Linfeng Lan[3,a)] and Xingqiang Liu,[1,2,a)]

[1]Key Laboratory for Micro/Nano Optoelectronic Devices of Ministry of Education& International Science and Technology Innovation Cooperation Base for Advanced Display Technologies of Hunan Province, School of Physics and Electronics, Hunan University, Changsha 410082, China.

[2]State Key Laboratory for Chemo/Biosensing and Chemometrics, College of Semiconductors (College of Integrated Circuits) Hunan University, Changsha 410082, China.

[3]School of Materials Science and Engineering, South China University of Technology, Guangzhou 510640, China.

[4]School of Materials Science and Engineering, Hunan University, Changsha 410082, China.

[5]Institute of Information and Communication Technologies, Electronics and Applied Mathematics, Université catholique de Louvain, Louvain-la-Neuve 1348, Belgium.

[6]Departament d'Enginyeria Electrònica, Elèctrica i Automàtica, Universitat Rovira i Virgili, 43007 Tarragona, Spain.

[a)] Authors to whom correspondence should be addressed:

Lei Liao, liaolei@whu.edu.cn; Linfen Lan, lanlinfeng@scut.edu.cn; Xingqiang Liu,

liuxq@hnu.edu.cn.

Abstract

The trade-off between mobility and stability in oxide thin-film transistors (TFTs) hinders further advances of active-matrix flat panel display. Herein, a solution-processed bilayer active channel is designed to improve the stability and mobility simultaneously. The optical bandgap and work function of Tb:In_2O_3 films are modulated by tuning the films thickness and Tb concentration of Tb-doped indium oxide (Tb:In_2O_3) films. Large conduction band offset is achieved in Tb:In_2O_3 bilayer channel, which induces accumulation of abundant electrons at the interface. The mobility is significantly improved to 38.2 cm^2/Vs, and the photoinduced stability of bilayer Tb:In_2O_3 TFTs is improved with low threshold voltage shift of 0.26 V and −0.38 V under negative-bias illumination stress (NBIS) and negative-bias temperature illumination stress (NBTIS), respectively.

Thin-film transistors (TFTs) based on oxide semiconductors are promising for active-matrix flat panel displays applications,[1-6] due to superior carrier mobility, low leakage current, and large-area uniformity.[7-9] However, the trade-off between mobility and stability limits further commercial applications of oxide TFTs in ultra-high resolution display technologies.[10] Moreover, the oxide TFTs present inferior reliability and stability when apply a negative gate bias stress combined with continuous light irradiation (NBIS) even in visible spectra region.[11,12]

Suppressing oxygen vacancies (V_O) concentration and widening the band gap of

oxide semiconductors are efficient to enhance the NBIS stability of oxide TFTs.[13-16] However, according to the percolation transport mechanism, the mobility and carrier concentration are proportional to V_O concentration in oxide semiconductors. Therefore, the decrement of V_O concentration would result in low carrier concentration and low mobility. It is an alternative strategy to improve the mobility of oxide TFTs by using a bilayer active channel configuration with appropriate band alignment.[17-20] As previously reported, by using an In_2O_3/ZnO bilayer channel with large conduction band (CB) offset, the electrons are confined on the plane of the atomically sharp heterointerface and give rise to a high mobility of 45 cm^2/Vs.[20] However, the NBIS stability of oxide TFTs based on bilayer channel is rarely reported.

Terbium (Tb) ions are employed as blue light down-conversion medium to improve NBIS stability of oxide TFTs because of the charge transfer transition between Tb ions and ligand ions.[21] Herein, bilayer Tb:In_2O_3 channel based on different Tb concentrations and film thicknesses is deposited by spin-coating aqueous solution. By controlling the thickness and Tb concentration in Tb:In_2O_3 bilayer thin films, the band alignment readily modulated with large CB offset, which contributes to electrons accumulation at the bilayer-channel interface and affords to improved mobility. The bilayer Tb:In_2O_3 TFTs continuously exhibit increased mobility of 38.2 cm^2/Vs, low subthreshold swing (SS) of 0.27 V/dec, desirable threshold voltage (V_{th}) of 0.1 V and high on/off ratio of 5×10^7. Meanwhile, the photoinduced stability of oxide TFTs is further improved, corresponding to a low V_{th} shift of 0.26 V and −0.38

V under NBIS and NBTIS, respectively. The strategy is potential to overcome the trade-off between mobility and stability in oxide TFTs.

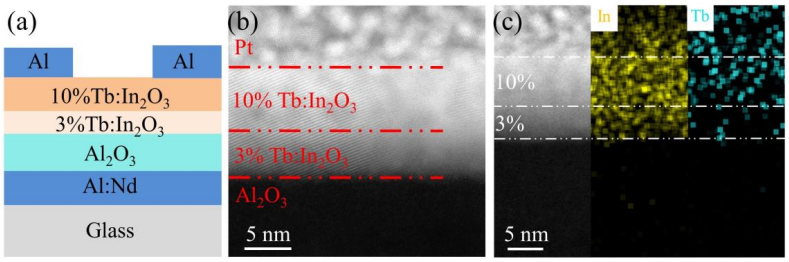

FIG. 1. (a) Structure diagram of bilayer $Tb:In_2O_3$ TFTs. (b) High-resolution cross-sectional TEM images and (c) EDS mapping image of bilayer $Tb:In_2O_3$ TFTs.

Figure 1(a) illustrates the schematic image of the bilayer $Tb:In_2O_3$ TFTs. The sputtering Al:Nd alloy and anodized Al_2O_3:Nd are employed as gate electrode and dielectric, respectively. The bilayer $Tb:In_2O_3$ films with different Tb concentrations stack on Al_2O_3:Nd are used as the active layers by spin-coating in sequence without passivation. Ultraviolet light irradiation is used to define wettable region by shadow mask for aqueous precursor deposition. The underneath $Tb:In_2O_3$ layer is deposited by spin-coating a 0.2 M precursor aqueous solution with 3% Tb content at 6500 rpm, followed by annealing at 300°C for 1 h in ambient conditions (relative humidity $\approx$ 70%). After oxygen plasma treatment for 50 s, a 0.3 M precursor aqueous solution with 10% Tb content is used to deposit the above active layer with the same procedure. Finally, thermally evaporated Al is used as the source/drain electrodes. Figure 1(b) shows the high-angle annular dark-field scanning transmission electron microscopy (HAADF-STEM) image of bilayer $Tb:In_2O_3$ channel. A 12 nm crystal

bilayer channel is obtained, which composes of two homogeneous Tb:In_2O_3 layers with 3% and 10% Tb content. Interestingly, the 3% and 10% Tb:In_2O_3 layer exhibit same grain orientation because of approximate ionic radius between In and Tb, which effectively reduce the interface-defects electron scattering effects. Figure 1(c) illustrates the element distributions of the bilayer Tb:In_2O_3 channel, indicating distinctly different Tb concentration in the bilayer channel. For EDS mapping, the signal of Pt is coincident with In and Tb, which is not diffusion of In and Tb.

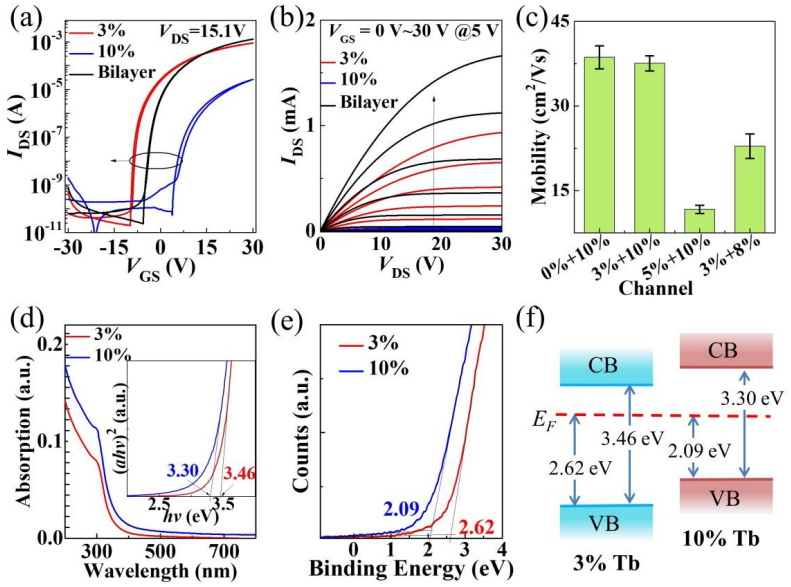

FIG. 2. (a) Transfer characteristics and (b) Output characteristics of Tb:In_2O_3 TFTs based on single layer and bilayer Tb:In_2O_3. (c) Statistical chart of Tb:In_2O_3 TFTs with different channels. (d) UV-visible absorption spectra of Tb:In_2O_3 films. (e) XPS valence band spectra of Tb: In_2O_3 films. (f) Energy band alignment of the Tb:In_2O_3 bilayer channel.

The transfer characteristics of Tb:In_2O_3 TFTs based on different channels are shown in Fig. 2(a). All devices exhibit typical n-type behavior and low off-state current. The effect of Tb-doped concentration on electronic characteristics of single-layer Tb:In_2O_3 TFTs is investigated. The evolution of mobility versus Tb concentration is shown in Figs. S1 and S2. It is worth noting that the single-layer Tb:In_2O_3 TFTs with 3% Tb concentration exhibit a saturation mobility (μ_{sat}) of 19.3 cm^2/Vs, which is equal to μ_{sat} of pure In_2O_3 TFTs (20.7 cm^2/Vs, see in Fig. S2). A small amount of Tb content would not affect overlaying of In 5*s* orbitals, so the on-state current and mobility are slightly decreased. However, as the carriers in oxide thin film mainly originate from oxygen vacancy (V_O), and the mobility is proportional to carrier density, excess Tb content would suppress V_O concentration and further results in poor channel current and mobility (Fig. S3). The μ_{sat} of single-layer Tb:In_2O_3 TFTs with 10% Tb sharply decline to 1.7 cm^2/Vs with a V_{th} (the intersection voltage between the linear part of the $I_{DS}^{1/2}$-V_{GS} curve and the V_{GS} axis) of 8.9 V. Therefore, excess Tb content would cause extremely low free carrier concentration. Moreover, positive hysteresis is observed in transfer curve of single-layer 10% Tb:In_2O_3 TFTs, which may be attributed to the generation of electron traps. On the other hand, as shown in Fig. 2(a), due to the accumulation of electrons at the homogeneous bilayer interface, the bilayer TFTs present improved performance with negligible hysteresis when compared with the single-layer Tb:In_2O_3 TFTs. And a high mobility of 38.2 cm^2/Vs is achieved in the 3%/10% bilayer Tb:In_2O_3 TFTs, which is ~2 and 22 times higher than single-layer 3% and 10% devices, respectively. Moreover,

the V_{th} of bilayer TFTs is more positive than that of 3% Tb:In_2O_3 TFTs, indicating the electron concentration is not increase in bilayer channel. Figure 2(b) shows typical output characteristics of Tb:In_2O_3 TFTs based on single-layer and bilayer channels. All devices exhibit obvious linear region and saturation region, suggesting quasi-ohmic contact, and the bilayer Tb:In_2O_3 TFTs exhibit improved output current. Fig. 2(c) plots the mobility distribution of bilayer Tb:In_2O_3 TFTs with different configurations ranged by Tb concentration. The 0% + 10% Tb:In_2O_3 bilayer channel TFTs also exhibit a high mobility of 42 cm^2/Vs, but a high off-state current (~10^{-7} A) due to excess electrons concentration (Fig. S5).

Energy band alignment will influence the electron distribution in bilayer oxide channel and further influence the device mobility. Therefore, the band structure of Tb:In_2O_3 films with 3% and 10% Tb concentrations are extracted. Figure 2(d) shows the UV-visible absorption spectra of Tb:In_2O_3 films. The 10% Tb:In_2O_3 film exhibits stronger absorption than 3% Tb:In_2O_3 film in blue spectrum region, because of strong charge transfer transition of TbO_X. Accordingly, the 3% Tb:In_2O_3 film have wider optical band gap as indicated by Tauc analysis:[22]

$$\alpha h\upsilon = C(h\upsilon - E_G)^b \quad (1)$$

where α is the optical absorbance, $h\upsilon$ is the incident photon energy, C is a constant, and b depends on the nature of semiconductor bandgap (1/2 is used for direct bandgap semiconductors). The inset in Fig. 2(d) shows the corresponding $(\alpha h\upsilon)^2$ *versus* $h\upsilon$ curves. The extracted optical bandgap is 3.46 eV and 3.30 eV for 3% and 10% Tb:In_2O_3 films, respectively. On the other hand, the optical bandgap of Tb:In_2O_3 films

would be widened by reducing the thickness when the thickness is below 20 nm.[23,24] And the bandgap difference (ΔE_G) can be calculated as:[25]

$$\Delta E_G = \frac{h^2}{8L^2}\left(\frac{1}{m_e^*} + \frac{1}{m_h^*}\right) \quad (2)$$

where h is Planck Constant, m_e^* and m_h^* are the effective masses of the electron and hole in the semiconductor, respectively, and L is the thickness of the semiconductor.

As aforementioned, the electron concentration in Tb:In_2O_3 film is dramatically decreased when Tb content increases from 3% to 10%. Therefore, a small conduction band minimum (CBM) difference between 3% and 10% Tb:In_2O_3 will cause drastic band bending at the bilayer interface to improve the mobility of TFTs. Figure 2(e) depicts the XPS valence band spectra of 3% and 10% Tb:In_2O_3 films. A difference between Fermi level (E_F) and VBM is 2.62 eV and 2.09 eV for 3% and 10% Tb:In_2O_3 films, respectively, which is attributed to the downward Fermi level due to lowing electron concentration as increase Tb content. The energy band alignment of the Tb:In_2O_3 bilayer with different Tb contents is described in Fig. 2(f). Large CB offset between 3% and 10% Tb:In_2O_3 films can promote the accumulation of electrons at the bilayer-channel interface, which affords to improved mobility in bilayer Tb:In_2O_3 TFTs. In addition, the barrier of CB between 3% and 10% Tb:In_2O_3 layer can effectively control the V_{th} and off current.

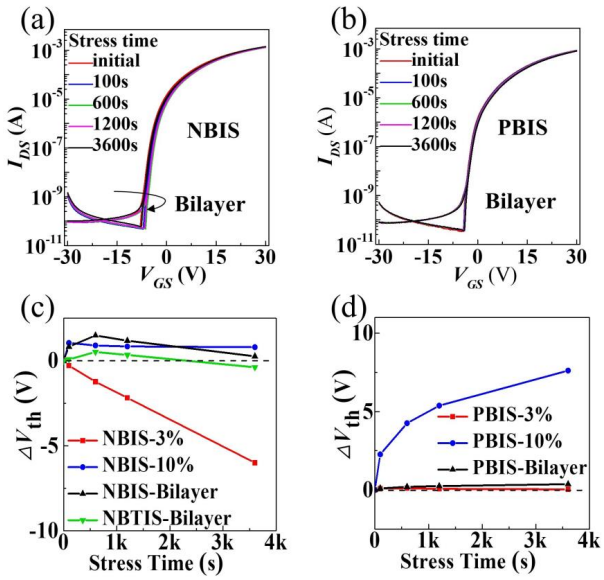

FIG. 3. Variations of time-dependent transfer curves of the bilayer TFTs under (a) PBIS and (b) NBIS. Detailed plot of V_{th} shift of TFTs with different channel as a function of stress time under (c) PBIS and (d) NBIS.

Figure 3(a) and (b) present the evolutions of the transfer curves of bilayer Tb:In_2O_3 TFTs as a function of the stress time under NBIS and PBIS without any passivation. The gate bias stresses of ±20 V combined with 250 Lux white light irradiation are used for PBIS and NBIS measurements under vacuum. Compared with pure In_2O_3 TFTs, Tb:In_2O_3 TFTs with 3% content have robust NBIS stability and acceptable mobility. However, the improved V_{th} shift (−6.0 V) is still insufficient for active-matrix displays. The NBIS stability is further improved with increment of Tb content, and a V_{th} shift of 0.9 V is obtained for 10% Tb:In_2O_3 TFTs in spite of a more

narrow band gap (Fig. 2d and 3c). The results indicate that high concentrations of Tb ions can effectively suppress the generation of V_O^{2+} under NBIS due to charge transfer transition. Whereas a poor PBIS stability with a V_{th} shift of 7.6 V is obtained (Fig. 3d), which is attributed to electron traps at dielectric/channel interface. Compared to single layer Tb:In_2O_3 TFTs, the bilayer Tb:In_2O_3 TFTs exhibit much better photoinduced stability with low V_{th} shift of 0.26 V and 0.37 V under NBIS and PBIS for 3600 s, respectively, as shown in Fig. 3(a) and (b). Interestingly, the transfer curves of bilayer TFTs slightly shift toward positive at the initial stage (before 600s) then shift backward to the negative direction (Fig. 3c). The positive shift of V_{th} may result from the charge transfer transition between Tb ion and oxygen ion or V_O under NBIS.[21] Due to existence of abundant trivalent and tetravalent Tb ion in 10% Tb:In_2O_3 layer, the delocalize electrons from V_O would be trapped by tetravalent Tb ion through charge transfer transition, even generating the interstitial oxygen, which result in positive shift of V_{th}.[26,27] Briefly, the superior NBIS stability of bilayer Tb:In_2O_3 TFTs is major attributed to: 1) the increased Tb content suppresses V_O photoionization; 2) self-compensation effect between 3% and 10% Tb:In_2O_3 layer decreases the defects density in bilayer channel interface;[28] 3) high-density free electrons confined at interface of bilayer channel due to CB offset, which is free from the influence of external impurities.

Besides illumination, the TFTs also inevitably suffer from the heat generated in the display circuits. Therefore, the stability under NBTIS is particularly important for oxide TFTs. The electron donations from carbon-monoxide-related impurities greatly

affect the stability of high-mobility oxide TFTs.[10] In this work, an aqueous solution is used to avoid the introduction of carbon-related impurities and improve the NBTS of oxide TFTs.[29] Therefore, the stability under NBTIS of bilayer Tb:In_2O_3 TFTs is tested at 60°C temperature, and a low V_{th} shift of −0.38 V is obtained (Fig. 3c).

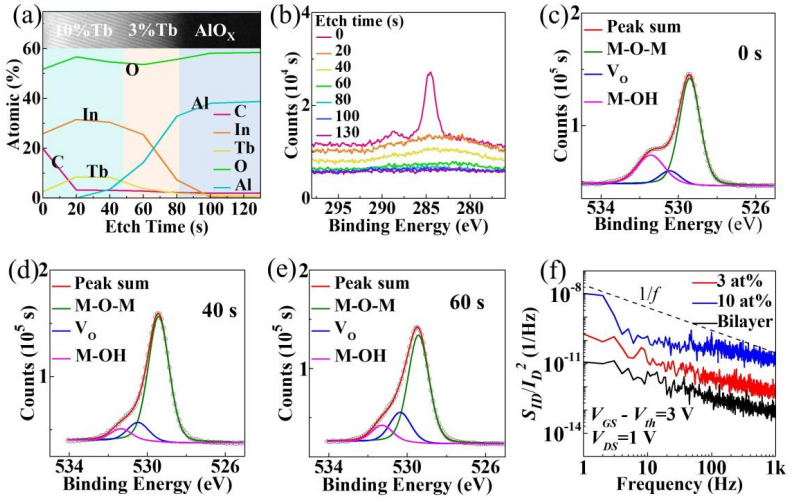

FIG. 4. (a) Elemental depth profile of the bilayer Tb:In_2O_3 channel stack on Al2O3 (inset is corresponding HRTEM image). (b) C1s spectra of bilayer channel at different etch time. O1*s* XPS spectra of bilayer channel with an etching time of (c) o s, (d) 40 s and (e) 60 s. (f) Normalized drain-current noise spectral density (S_{ID}/I_D^2) dependence of frequency.

In order to further investigate defect characteristics of Tb:In_2O_3 bilayer channel, XPS depth profile is carried out. Figure 4(a) shows the depth-resolved elemental composition of the bilayer channel stack on Al_2O_3. The oxygen-elemental composition exhibits a minimal value at an etching time of 60 s, corresponding to 3% Tb:In_2O_3 layer with higher V_O ratio obtained by fitting O 1s spectrum. As shown in

Fig. 4(b), the carbon elemental is only detected on the surface of bilayer channel, which is consistent with the O 1*s* spectra at varying etch time (depth) that signal intensity with binding energy at around 532 eV related carbon impurities in bulk of bilayer is decreased significantly compared to surface.[10,30] The results indicate that aqueous solution could effectively avoid introduction of carbon-related impurities and 10% Tb:In_2O_3 layer of low carrier concentration separate high-speed electron transport layer (3% Tb:In_2O_3 layer) from carbon-related impurities absorbed on surface of bilayer channel, resulting in improvement of NBTS stability. The O 1*s* spectra at different etch time are fitted by three Gaussian distributions with binding energies at 529.4 eV, 530.4 eV and 531.4 eV, corresponding to the oxygen in oxide lattices (M–O–M), oxygen vacancies (V_O) and metal hydroxide (or loosely bound oxygen) species (M–OH),[31] respectively, as shown in Fig. 4(c-e). The interior of bilayer channel shows lower metal hydroxide ratio than that of surface without etching. With etching time increasing from 20 s, 40 s to 60 s, the V_O ratio are 7.9%, 11.8%, and 19.0%, respectively. A low V_O ratio is obtained at an etching time of 40 s near the interface of bilayer channel, which may be attributed to the defect self-compensation effect. Low hydroxide ratio and high M–O–M ratio also provide a high-quality interface for improving the mobility. As a result, the deposition of 10% Tb:In_2O_3 layer can effectively remove the carbon- and hydroxide-related impurities adsorption, and improve the NBT/IS stability.

Low frequency noise (LFN) is used to characterize the traps density of oxide TFTs with different channel configurations.[32] The relationship between normalized

drain-current noise spectral density (S_{ID}/I_D^2) and frequency (ranges from 5 to 1000 Hz) for oxide TFTs at V_{GS}–V_{th} = 3 V and V_{DS} = 1 V is shown in Fig. 4(f). It is clear that bilayer Tb:In_2O_3 TFTs show a lowest S_{ID}/I_D^2 and fit classical 1/*f* noise theory, indicating decreased average trap density within the bilayer channel region.

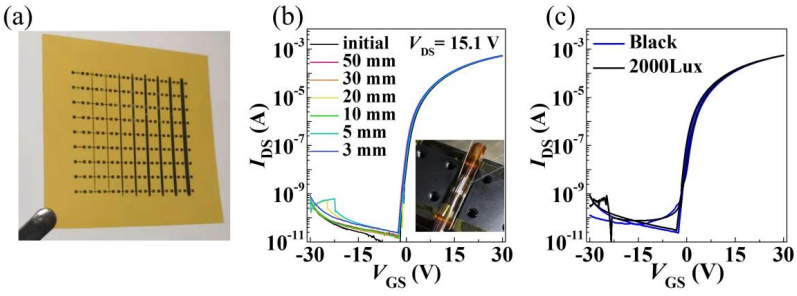

FIG. 5. (a) Photograph of the actual transistors fabricated on a flexible polyimide (PI) substrate. (b) Transfer characteristics with varying bending radius. (c) Photoresponse of devices at the bending radius of 3 mm.

Finally, the processed temperature of bilayer Tb:In_2O_3 TFTs is below 300°C, which is greatly potential for flexible electronics. A large-area flexible array is fabricated on polyimide (PI) substrate with an annealing temperature of 280°C, as shown in Fig. 5(a). And Fig. 5(b) describes typical transfer characteristics at different bending radius. Slightly parallel shift of transfer curves with 4.8% mobility increment is observed as bending, indicating good flexibility. The flexible devices exhibit low photo-sensitivity even at the bending radius of 3 mm, as shown in Fig. 5(c). The results prove the bilayer Tb:In_2O_3 TFTs are promising for flexible display technology.

In summary, in order to overcome the trade-off between mobility and stability of

oxide TFTs, a bilayer channel consist of Tb incorporated In_2O_3 with different content is rationally designed. High-performance oxide TFTs based on bilayer Tb:In_2O_3 channel are fabricated with robust mobility and reliability by accurately modulating Tb concentration. The bilayer Tb:In_2O_3 TFTs exhibit a mobility value of 38.2 cm^2/Vs and a low threshold voltage shifts of 0.26 V and –0.38 V under NBIS and NBTIS, respectively.

See the supplementary material for the electrical performances and XPS O-1s spectra of single-layer Tb:In_2O_3 TFTs, and transfer characteristics of bilayer Tb:In_2O_3 TFTs.

ACKNOWLEDGMENTS

The authors are deeply grateful to the Special Support from China Postdoctoral Science Foundation (No. 2021TQ0100), the National Key Research and Development Program of Ministry of Science and Technology (No. 2018YFA0703704), the National Natural Science Foundation of China (Nos. 61851403 and 51872084), the National Funds for Distinguished Young Scientists (No. 61925403), the Natural Science Foundation of Hunan Province (No. 2020JJ1002), and the Key Research and Development Program of Hunan Province (No. 2022WK2001).

Data Availability

The data that support the findings of this study are available from the corresponding author upon reasonable request

Conflict of interest

The authors have no conflicts to disclose.

REFERENCES:

[1]K. Nomura, H. Ohta, A. Takagi, T. Kamiya, M. Hirano, and H. Hosono, Nature **432**, 488 (2004).
[2]S. M. Kwon, J. Y. Kwak, S. Song, J. Kim, C. Jo, S. S. Cho, S. J. Nam, J. Kim, G. S. Park, Y. H. Kim, and S. K. Park, Adv. Mater. **33**, 2105017 (2021).
[3]S. Wei, F. Wang, X. Zou, L. Wang, C. Liu, X. Liu, W. Hu, Z. Fan, J. C. Ho, and L. Liao, Adv. Mater. **32**, 1907527 (2019).
[4]S. Jeon, S. Ahn, I. Song, C. J. Kim, U. Chung, E. Lee, I. Yoo, A. Nathan, S. Lee, K. Ghaffarzadeh, J. Robertson, and K. Kim, Nat. Mater. **11**, 301 (2012).
[5]G. Yang, C. Chen, F. Yao, Z. Chen, Q. Zhang, X. Zheng, J. Ma, H. Lei, P. Qin, L. Xiong, W. Ke, G. Li, Y. Yan, and G. Fang, Adv. Mater. **30**, 1706023 (2018).
[6]D. Zheng, G. Wang, W. Huang, B. Wang, W. Ke, J. L. Logsdon, H. Wang, Z. Wang, W. Zhu, J. Yu, M. R. Wasielewski, M. G. Kanatzidis, T. J. Marks, and A. Facchetti, Adv. Funct. Mater. **29**, 1900265 (2019).
[7]H. Zan, C. Yeh, H. Meng, C. Tsai, and L. Chen, Adv. Mater. **24**, 3509 (2012).
[8]S. Z. Bisri, C. Piliego, J. Gao, and M. A. Loi, Adv. Mater. **26**, 1176 (2014).
[9]C. Chen, B. R. Yang, G. Li, H. Zhou, B. Huang, Q. Wu, R. Zhan, Y. Y. Noh, T. Minari, S. Zhang, S. Deng, H. Sirringhaus, and C. Liu, Adv. Sci. **6**, 1801189 (2019).
[10]Y. Shiah, K. Sim, Y. Shi, K. Abe, S. Ueda, M. Sasase, J. Kim, and H. Hosono, Nat. Electron. **4**, 800 (2021).
[11]J. K. Jeong, H. Won Yang, J. H. Jeong, Y. Mo, and H. D. Kim, Appl. Phys. Lett. **93**, 123508 (2008).
[12]T. Kamiya, K. Nomura, and H. Hosono, Sci. Technol. Adv. Mat. **11**, 44305 (2016).
[13]B. S. Yang, S. Park, S. Oh, Y. J. Kim, J. K. Jeong, C. S. Hwang, and H. J. Kim, Journal of Materials Chemistry **22**, 10994 (2012).
[14]K. H. Ji, J. Kim, H. Y. Jung, S. Y. Park, R. Choi, U. K. Kim, C. S. Hwang, D. Lee, H. Hwang, and J. K. Jeong, Appl. Phys. Lett. **98**, 103509 (2011).
[15]J. Li, Y. Fu, C. Huang, J. Zhang, X. Jiang, and Z. Zhang, Appl. Phys. Lett. **108**, 143505 (2016).
[16]J. Kim, J. Bang, N. Nakamura, and H. Hosono, APL Mater. **7**, 22501 (2019).
[17]H. Faber, S. Das, Y. H. Lin, N. Pliatsikas, K. Zhao, T. Kehagias, G. Dimitrakopulos, A. Amassian, P. A. Patsalas, and T. D. Anthopoulos, Sci. Adv. **3**, e1602640 (2017).
[18]Y. Chen, W. Huang, V. K. Sangwan, B. Wang, L. Zeng, G. Wang, Y. Huang, Z. Lu, M. J. Bedzyk, M. C. Hersam, T. J. Marks, and A. Facchetti, Adv. Mater. **31**, 1805082 (2019).

[19]M. Lee, J. Jo, Y. Kim, S. Choi, S. M. Kwon, S. P. Jeon, A. Facchetti, Y. Kim, and S. K. Park, Adv. Mater. **30**, 1804120 (2018).
[20]J. Yang, J. H. Choi, S. H. Cho, J. Pi, H. Kim, C. Hwang, K. Park, and S. Yoo, IEEE Electron Device Lett. **39**, 508 (2018).
[21]P. He, H. Xu, L. Lan, C. Deng, Y. Wu, Y. Lin, S. Chen, C. Ding, X. Li, M. Xu, and J. Peng, Commun. Mater. **2,** 86 (2021).
[22]J. Tauc, R. Grigorovici, and A. Vancu, Phys. Status Solidi B. **15,** 627 (1966).
[23]Y. Lin, H. Faber, J. G. Labram, E. Stratakis, L. Sygellou, E. Kymakis, N. A. Hastas, R. Li, K. Zhao, A. Amassian, N. D. Treat, M. McLachlan, and T. D. Anthopoulos, Adv. Sci. **2**, 1500058 (2015).
[24]J. G. Labram, Y. Lin, K. Zhao, R. Li, S. R. Thomas, J. Semple, M. Androulidaki, L. Sygellou, M. McLachlan, E. Stratakis, A. Amassian, and T. D. Anthopoulos, Adv. Funct. Mater. **25**, 1727 (2015).
[25]R. Dingle, W. Wiegmann, and C. H. Henry, Phys. Rev. Lett. **33**, 14 (1974).
[26]H. Zhu, C. Yang, Q. Li, Y. Ren, J. C. Neuefeind, L. Gu, H. Liu, L. Fan, J. Chen, J. Deng, N. Wang, J. Hong, and X. Xing, Nat. Commun. **9,** 5063 (2018).
[27]R. K. Verma, K. Kumar, and S. B. Rai, Solid State Sci. **12**, 1146 (2010).
[28]J. He, G. Li, Y. Lv, C. Wang, C. Liu, J. Li, D. Flandre, H. Chen, T. Guo, and L. Liao, Adv. Electron. Mater. **5**, 1900125 (2019).
[29]M. Li, W. Zhang, W. Chen, M. Li, W. Wu, H. Xu, J. Zou, H. Tao, L. Wang, M. Xu, and J. Peng, ACS Appl. Mater. Interfaces **10**, 28764 (2018).
[30]A. R. Gonzalez-Elipe, J. P. Espinos, A. Fernandez, and G. Munuera, Appl. Surf. Sci. **45**, 103 (1990).
[31]S. W. Cho, D. E. Kim, W. J. Kang, B. Kim, D. H. Yoon, K. S. Kim, H. K. Cho, Y. Kim, and Y. Kim, J. Mater. Chem. C **5**, 339 (2017).
[32]F. N. Hooge, IEEE Trans. Electron Devices **41**, 1926 (1994).

PLEASE CITE THIS ARTICLE AS DOI: 10.1063/5.0098765

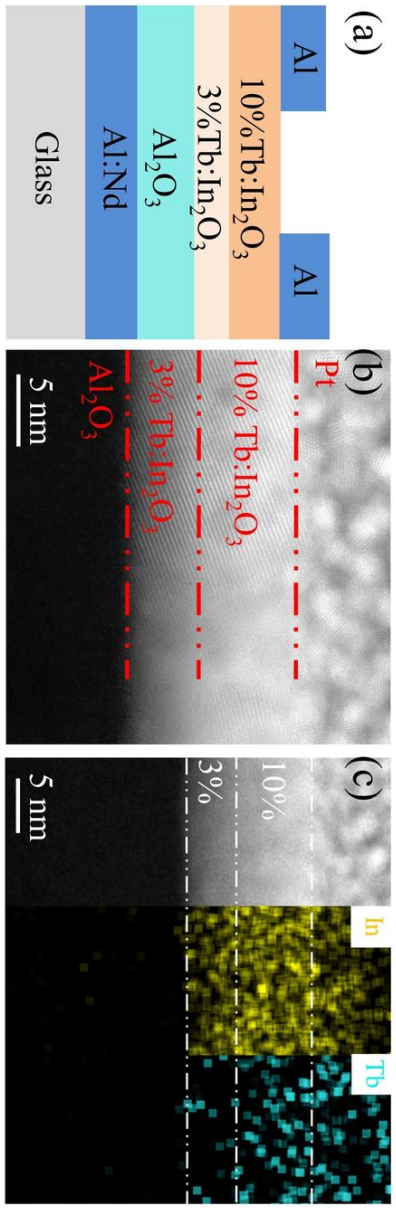

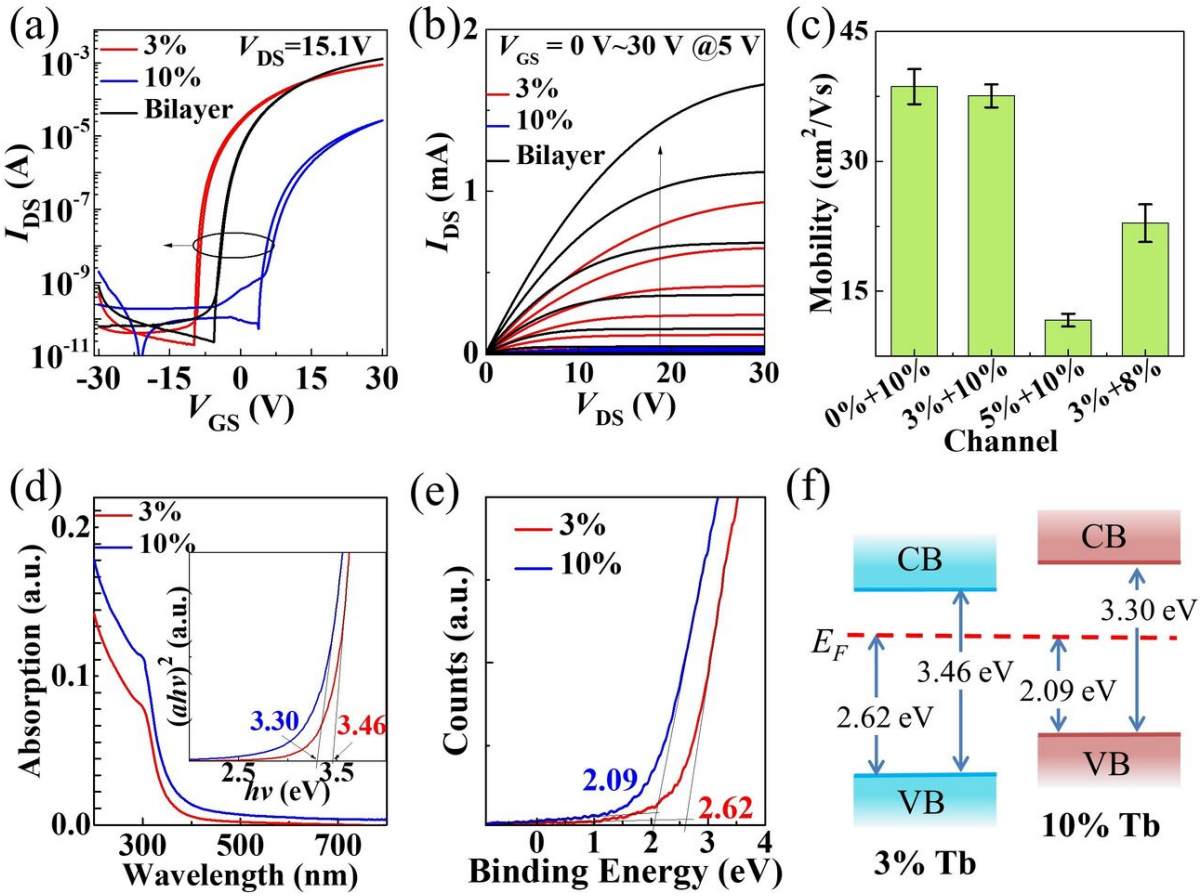

PLEASE CITE THIS ARTICLE AS DOI: 10.1063/5.0098765